Paper No.
2406

NACE INTERNATIONAL CORROSION 2013 CONFERENCE & EXPO

ELECTROCHEMICAL STUDY AND MODELING OF H_2S CORROSION OF MILD STEEL

Yougui Zheng, Bruce Brown, Srdjan Nesic
Institute for Corrosion and Multiphase Technology
Department of Chemical and Biomolecular Engineering
Ohio University
342 W. State St.
Athens, OH 45701

ABSTRACT

The internal corrosion of mild steel in the presence of hydrogen sulfide (H_2S) represents a significant challenge in oil production and natural gas treatment facilities, but the true mechanisms involved in H_2S corrosion are still not fully understood. The lack of knowledge makes the prediction, prevention and/or control of aqueous H_2S corrosion of mild steel much more difficult. In the present study H_2S corrosion mechanisms were experimentally investigated in short term corrosion tests (1-2hr), conducted in 1 wt% NaCl solution at different pH (pH2 to pH5), at different temperature (30°C to 80°C), under various H_2S/N_2 concentration ratios (0-10%) and flow rates, using a X65 mild steel rotating cylinder electrode. Corrosion rates were measured by linear polarization resistance (LPR). Corrosion mechanisms were investigated by using potentiodynamic sweeps and by comparison with electrochemical modeling. LPR results showed that corrosion rates increased with increasing temperature, partial pressure of H_2S, flow rate and decreasing pH. Results of potentiodynamic sweeps show the presence of H_2S could affect both cathodic reactions and the anodic reaction. A new electrochemical model was developed and can be used to predict the effect of temperature, pH, pH_2S and flow on corrosion mechanisms of mild steel in aqueous solutions containing H_2S.

Key words: hydrogen sulfide, electrochemical mechanism, model.

INTRODUCTION

The corrosion of mild steel by H_2S containing media has been investigated since the 1940s.[1] Recently more attention was focused on this type of corrosion because of harsher environments encountered when exploring new sources of oil and gas, which usually contain H_2S. The understanding, prediction, and control of H_2S corrosion are some of the key challenges for oil and gas production. Despite the relative abundance of experimental data on H_2S corrosion of mild steel, most of the literature is still confusing and somewhat contradictory. Therefore the mechanism of H_2S corrosion remains much less understood when compared to that of CO_2 corrosion. Moreover, in most cases, the formation of iron sulfide layers plays a key role in governing H_2S corrosion. The complex mechanism of iron sulfide

formation makes it difficult to quantify the H_2S corrosion rate.[2-6] Some critical studies of H_2S corrosion are outlined below.

Morris, *et al.*[7] used a mild steel rotating disc electrode (RDE) to study corrosion in aqueous solutions of acid pH (pH 3 to pH4) with H_2S. They found that the presence of H_2S shifted the anodic polarization curves of steel toward more negative potentials in weak acid solutions, with Tafel slopes of the anodic processes at ~ 0.041 V/decade. They also found that a limiting current density in an acidic solution gradually disappears as the concentration of H_2S increased. They concluded the process was under activation control and Tafel slope didn't change with H_2S, staying consistently in the range of 0.11 - 0.116 V/decade. They also found the corrosion reaction order with H_2S to be n = ($\partial \log i_{corr}/\partial \log [H_2S]$) = 0.2.

Iofa, *et al.*[8], also found acceleration effects of H_2S on the anodic reaction and attributed this effect to the chemisorptions and catalysis of H_2S. Shoesmith, *et al.*[2] also proposed a similar anodic reaction mechanism to Iofa's and suggested a solid state reaction for iron sulfide formation. Cheng *et al.*[9] found the anodic dissolution current (i_a) increased with pH and H_2S concentration with reaction orders of about $n_{pH} = n_{H2S} = 0.25$ and i_{corr} increased with $[H_2S]$ by a reaction order $nH_2S = [\partial \log i_{corr}/\partial \log[H_2S])_{pH,E} = 0.20$ when $[H_2S]/[H_3O^+] < 10^{1.5}$. Recently, Sun and Nesic[10] proposed a mechanistic model based on a mass transfer control mechanism for corrosion in the presence of sulfide layers, often seen H_2S corrosion.

Despite many studies that have appeared in the literature, more questions still need to be answered regarding the effect of H_2S on mild steel corrosion. Some of the key ones are:

- is there an additional cathodic reaction – direct H_2S reduction? Direct H_2S reduction has been proposed by several authors, but direct evidence for its existence is still not available;
- how does the H_2S affect the anodic reaction of iron dissolution?
- what is the mechanism and kinetics of formation and growth of an FeS layer?
- how does an FeS layer affect the cathodic reactions and the anodic reaction?

The objective of the present work was to seek answers to the first two questions. Therefore an experimental study was organized where corrosion of mild steel was examined by electrochemical techniques, in short term experiments (before any iron sulfide layers formed), in solutions at various pH and different temperature, under various H_2S/N_2 concentration ratios and flow rates conditions, using an X65 mild steel rotating cylinder electrode. The third question was previously addressed by the work of Sun and Nesic[10] and is currently being scrutinized. The last question will be addressed in future work.

EXPERIMENTAL

Equipment

Experiments were conducted at atmospheric pressure in a 2 liter glass cell with a 1wt% NaCl in deionized water solution. Gas (mixture of hydrogen sulfide, H_2S and nitrogen, N_2) was sparged through the cell continuously. A three-electrode setup was used. A rotating cylinder electrode (RCE) with a speed control unit was used as the working electrode (WE). A platinum wire was used as a counter electrode (CE). A saturated silver-silver chloride (Ag/AgCl) reference electrode (RE) was connected to the cell externally *via* a Luggin capillary. The pH was monitored with an electrode immersed in the electrolyte. The concentration of H_2S was adjusted by a gas rotameter and measured by a gas sample pump with H_2S detector tubes. A carbon scrubber was used to treat the gas coming out of glass cell to remove the H_2S.

Material

X65 pipeline steel was tested. The composition of the X-65 steel (as reported by the manufacturer) used in the present experiments is shown in Table 1. The WE was machined from the parent steel material and had a diameter of 1.20 cm and a working surface area of 5.4 cm^2.

Table 1. Chemical composition of 5LX65 used in RCE (wt %).

Cr	Mo	S	V	Si	C	Fe	Ni	Mn	P
0.14	0.16	0.009	0.047	0.26	0.13	Balance	0.36	1.16	0.009

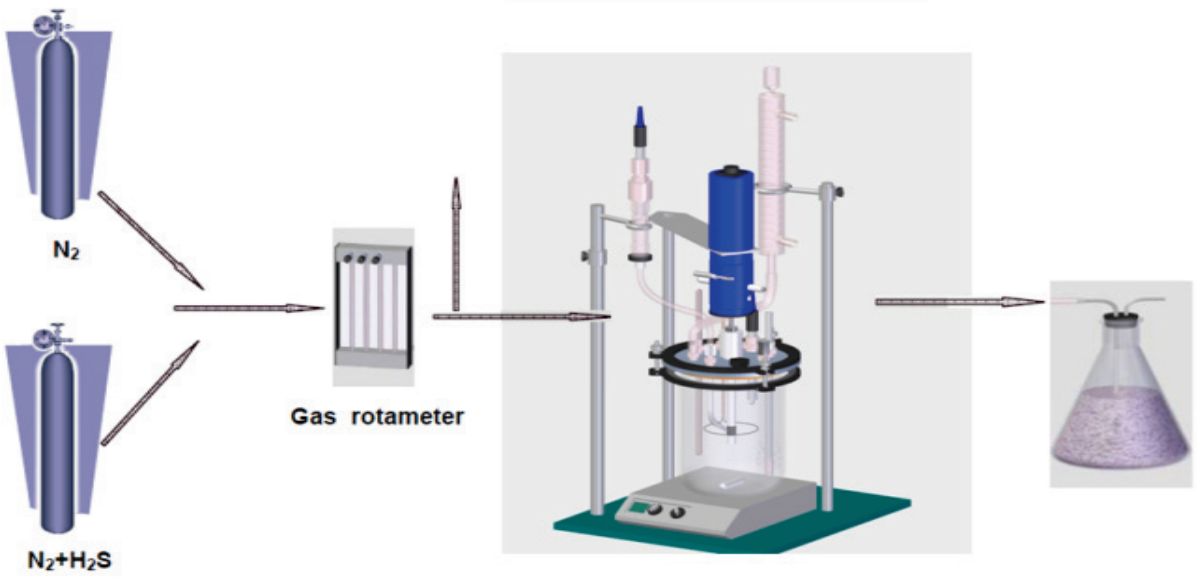

Figure 1. Schematic of the experimental cell.

Procedure

The aqueous solution was initially purged with N_2 gas for at least three hours to remove oxygen. After the solution was deoxygenated, H_2S was added by purging for at least half an hour to saturate the solution at the required partial pressure of H_2S. H_2S gas concentration was adjusted by purging different ratios N_2 and H_2S, from 100 ppm(v) to 10 %(v) H_2S, corresponding respectively to a H_2S partial pressure pH_2S = 0.1 mbar and 96.5 mbar, at 30°C. The pH was adjusted by adding deoxygenated hydrochloric acid or sodium hydroxide. Prior to immersion, the mild steel specimen surfaces were polished with 400 and 600 grit sandpaper, rinsed with alcohol and dried with an air blower.

Table 2. Experimental conditions.

Description	Parameters
Test Material	API 5L X-65
Test Solution	1 wt% NaCl Solution
Purged Gas(H_2S volume fraction in H_2S/N_2)	0 -10%(v) (0 – 0.1bar)
Rotating Speed / rpm	200 to 4000rpm
Total Pressure / bar	1
Temperature /°C	30°C, 60°C, 80°C
pH	2-5
Test Duration	0.5 to 2h
Measurement Methods	LPR, EIS, Potentiodynamic Sweeps, Weight Loss

Polarization resistance (R_p) measurements were conducted by polarizing the WE ± 5 mV from the free corrosion potential and scanning at 0.125 mV/s. Solution resistance was measured independently using electrochemical impedance spectroscopy (EIS), and the measured R_p then was corrected. The LPR constant B = 23 mV/decade used in this work was determined from longer term weight loss measurements. EIS measurements were carried out by applying an oscillating potential ± 5 mV around the free corrosion potential of the WE, using the frequency range 3 mHz to 5kHz. At the end of each experiment, the potentiodynamic sweeps were conducted at a sweep rate of 1 mV/s. The solution resistance was manually corrected for after the measurements. The test matrix for the experimental work is shown in Table 2.

RESULTS AND DISCUSSION

Effect of pH_2S

Effects of H_2S on polarization curves at different pH, and 1000rpm rotating speed condition are shown in Figure 2, Figure 3, and Figure 4. At pH4, the cathodic polarization curve for a pure N_2 purged environment without H_2S shows the typical characteristics, consisting of H^+ (proton) reduction and H_2O (water) reduction. A mass transfer limiting current plateau is observed. The Tafel slope of H_2O reduction is close to 120 mV /decade. The additions of 100ppm or 1000ppm H_2S do not change the cathodic polarization curves much, but they lower the H_2O reduction rate, which indicates a retardation effect possibly due to surface coverage by a sulfide species. The H_2O reduction rate in an H_2S environment is found to be generally 20 times lower than without H_2S. This retardation effect of H_2O reduction is observed at all experimental conditions with H_2S, even at a lower pH level, i.e. pH2, where iron sulfide should not be able to form. Therefore, the retardation effect of the H_2O reduction reaction is not considered to be related to iron sulfide formation.

At the same pH4, when 1% or 10% H_2S was introduced, the cathodic polarization curves show a second "wave" at more cathodic potential, which should be from the direct reduction of H_2S on the steel surface according to:

$$2H_2S(aq) + 2e^- \rightarrow H_2(g) + 2HS^-(aq) \quad (1)$$

Tests conducted at a higher pH5, could better distinguish the direct H_2S reduction from H^+ reduction more clearly. From Figure 3, at pH5 in a N_2 environment, the cathodic contribution from H^+ reduction becomes smaller and the direct H_2O reduction is the dominant cathodic reaction. The cathodic polarization curve appears almost as a straight line; no mass transfer limiting current plateau is observed. With 100ppm H_2S, the additional contribution from H_2S is still not clearly shown. However, in the presence of 10% H_2S, the contribution of H_2S reduction to the total corrosion current becomes dominant. The existence of an additional electrochemical reaction - direct H_2S reduction seems to be clear.

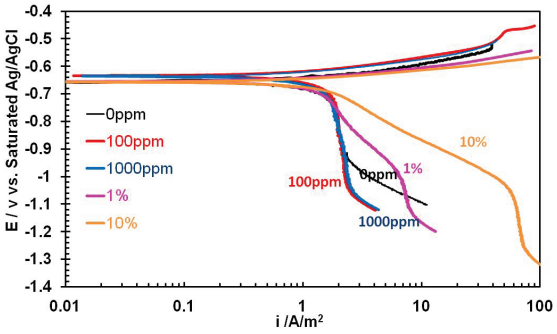

Figure 2. Effect of H_2S on polarization curves at pH4, 30°C, total pressure 1 bar, 1wt% NaCl, 1000rpm.

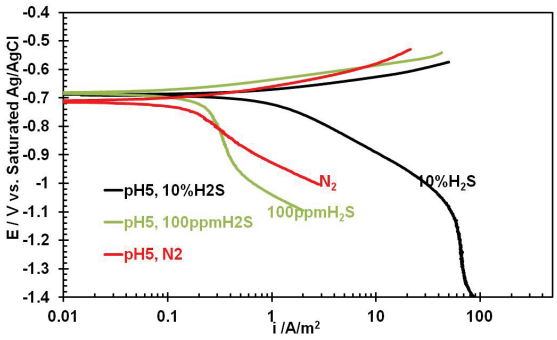

Figure 3. Effect of H_2S on polarization curves at pH5, 30°C, total pressure 1 bar, 1wt% NaCl, 1000rpm.

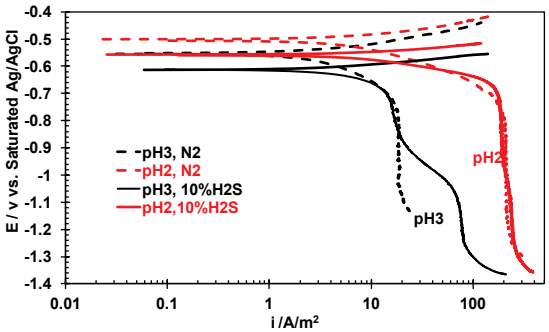

Figure 4. Effect of H_2S on polarization curves at pH3 and pH2, 30°C, total pressure 1 bar, 1wt% NaCl, 1000rpm.

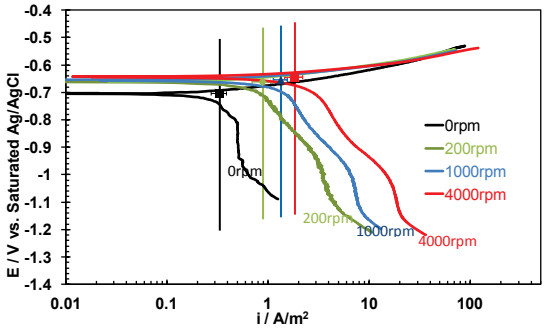

Figure 5. Effect of flow rate on polarization curves at 1% H_2S, pH4, 30°C, total pressure 1 bar, 1wt% NaCl. Vertical lines are LPR corrosion currents using B = 23 mV/ decade.

The effect of H_2S on the anodic iron dissolution reaction can also be seen in the polarization curves. At pH4 (Figure 2), with 100ppm and 1000pmm H_2S, the anodic polarization curves shift to the left as compared with N_2 environment, which indicates a retardation effect from H_2S. With 1% and 10% H_2S, the accelerating effect from H_2S is shown, as the anodic polarization curve shift to the right. The accelerating effect of H_2S on anodic reaction of iron dissolution can be observed more clearly from the anodic polarization curves at more acid conditions, pH2 and pH3 (Figure 4). This observation also agrees with the previous researchers.[7-9] The accelerating effect seems to be related to HS^- adsorption.

From the results discussed above, the presence of H_2S affects both anodic reaction and cathodic reaction. There is an effect of H_2S in anodic dissolution iron and an additional cathodic reaction: direct H_2S reduction.

Effect of Flow Rate

Effect of flow rate on the polarization curves for the 1% H_2S condition is shown in Figure 5. At this condition, the cathodic reactions are: H^+ reduction, direct H_2S reduction and H_2O reduction, which make two "waves" appear in the cathodic curve. Water reduction is under charge transfer control, which is flow independent. The reduction rates of H^+ and H_2S are influenced by the diffusion of reactants to the surface, so that, at a given flow rate, the total mass transfer limiting current i_{lim} for mild steel in an H_2S purged solution can be described by the additive contribution of two components:

$$i_{\lim} = i_{\lim,H^+} + i_{\lim,H_2S} \tag{2}$$

where $i_{lim,H+}$ and $i_{lim,H2S}$ are the limiting current densities in turbulent flow conditions for H^+ ions and $[H_2S]_{aq}$ molecules, respectively. For RCE, the $i_{lim,H+}$ can be calculated from Eisenberg expression [11]

$$i_{\lim,H^+} = 0.0791 F C_{H^+} d_{RCE}^{-0.30} \nu^{-0.344} D_{H^+}^{0.644} u_{RCE}^{0.7} \tag{3}$$

where $i_{lim,H+}$ is the limiting current density for H^+ reduction (A/m^2), F is the Faraday constant (96485 C/mol), C_{H^+} is the bulk concentration of protons (mol/m^3), d_{RCE} is the diameter of rotating cylinder (m), ν is the kinematic viscosity of the liquid (m^2/s), D_{H^+} is diffusion coefficient of protons (m^2/s), and u_{RCE} is the peripheral velocity of the RCE (m/s). The total limiting current density for H_2S, obtained from Figure

5, is found to be in good agreement with the theoretical mass transport limiting current for H_2S calculated using the Eisenberg expression:

$$i_{\lim,H_2S} = 0.0791FC_{H_2S}\, d_{RCE}^{-0.30} v^{-0.344} D_{H_2S}^{0.644} u_{RCE}^{0.7} \quad (4)$$

From Figure 5, the three anodic curves displayed clear Tafel behavior, with a slope of ≈ -40 -50 mV /decade. No effect of rotating speed on the anodic reaction was noticed, as expected.

Polarization curves for the solution purged with 10% H_2S at pH4 are shown in Figure 6. The overall shape of the curves was a slightly different compared to those in the experiments with 1% H_2S. The second "wave" on the cathodic polarization curves is not as clearly observed as it was at 1%H_2S. This is because the bulk concentration of H_2S is 10 times higher providing more cathodic current and thereby masks the "wave" from H^+ reduction. The mass transfer limiting current in this case is mostly attributed to the reduction of H_2S. The mass transfer limiting current density for H_2S obtained in this test is in good agreement with the prediction made by Eisenberg expression, Equation (4).

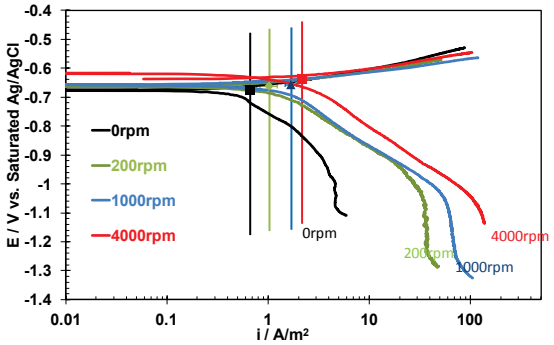

Figure 6. Effect of flow rate on polarization curves at 10% H2S , pH4, 30°C, total pressure 1 bar, 1% NaCl. Vertical lines are LPR corrosion currents using B = 23 mV/ decade.

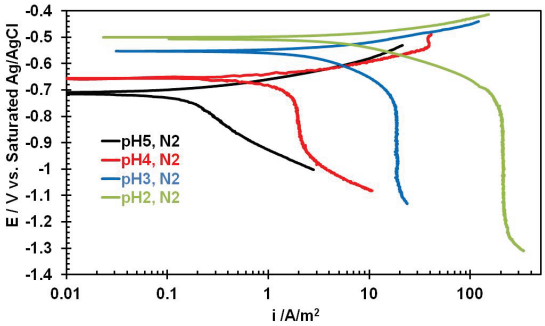

Figure 7. Effect of pH on polarization curves in the solution purged with N_2, 1000rpm, 30°C, total pressure 1 bar, 1wt% NaCl.

Both the tests at 1% H_2S and 10% H_2S confirmed that the direct reduction of H_2S is flow sensitive. The mass transfer limiting currents were observed and could be predicted by using mass-transfer correlations such as the correlation of Eisenberg, *et al.* for a rotating cylinder. Morris, *et al.* concluded that a limiting current density in an acidic solution gradually disappears as the concentration of H_2S increased.[7] But from review of their published data, it appears that they hadn't polarized the steel low enough (in the cathodic direction) to see the appearance of the mass transfer limiting current. The current work extends their results to show that the limiting current density does increase as the concentration of H_2S is increased.

Moreover, from Figure 5 and Figure 6, it is seen that the corrosion currents i_{corr} (vertical lines) are smaller than the mass transfer limiting currents, which indicated that the H_2S corrosion is not always under mass transfer control.

Effect of pH

Solution without H_2S

The effect of pH in a solution without H_2S is shown in Figure 7. The $i_{lim,H+}$ values at 1,000 rpm were reduced proportionately to the H^+ concentration with a tenfold change observed. The position of the Tafel line for H_2O reduction stayed approximately the same over the whole pH range, with a slope of≈ 120 mV/decade. This was in accordance with theory and agreed with the findings of Nesic, *et al.*[12]

The analysis of anodic polarization curves showed that the Tafel line for anodic dissolution of iron maintained the slope of 40 -50mV/decade over the whole pH range tested. The decrease of exchange current density was significant from pH 2 to pH 4 and much less between pH 4 and pH 5, which is in agreement with findings of Bockris, *et al.*[13]

Solution with H_2S

The effect of pH in a solution purged with 10% H_2S is shown in Figure 8. The decrease in limiting current is much less from pH3 to pH5 than expected for a tenfold decrease in H^+ concentration, if assuming that the cathodic reaction was solely H^+ reduction. The reason for that is that the main contribution for the cathodic limiting current from pH3 to pH5 is from the $[H_2S]_{aq}$ species, whose concentration is independent of pH value. However, at pH2 the main contribution for cathodic limiting current is from H^+, while a small "bump" on the limiting current plateau can still be observed due to the additional $[H_2S]_{aq}$.

From Figure 8, water reduction curve at 10% H_2S stayed approximately the same over the whole pH range, except at pH5 which was most likely caused by an experimental error.

Figure 8 also shows that pH had a smaller effect on the anodic dissolution reaction at 10% H_2S, especially from pH3 to pH5 which is different from the results obtained without H_2S. According to the finding of Cheng *et al.* [9], anodic dissolution current (i_a) is independent of pH and pH_2S when $[H_2S]_{aq}/[H^+] > 10^{1.5}$. As can be seen from the first dissociation of H_2S in solution:

$$H_2S(aq) \overset{K_{H_2S}}{\Leftrightarrow} H^+(aq) + HS^-(aq) \quad (5)$$

$$K_{H_2S} = \frac{[H^+][HS^-]}{[H_2S]} \quad (6)$$

Actually the ratio of $[H_2S]_{aq}/[H+]$ is equal to $[HS^-]/K_{H2S}$. Anodic dissolution current will reach a maxim value when HS^- exceeds a specific concentration at a specific temperature.

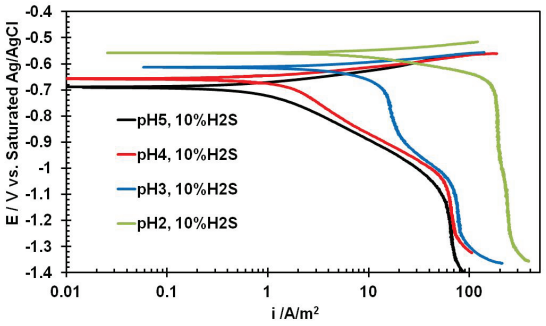

Figure 8. Effect of pH on polarization curves in the solution purged with 10%H_2S, 1000rpm, 30°C, total pressure 1 bar, 1wt% NaCl.

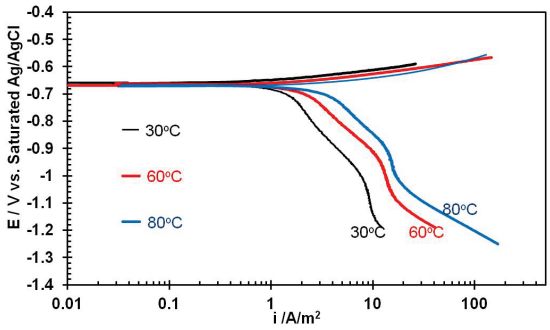

Figure 9. Polarization curves at pH4 for temperatures 30°C, 60°C, and 80°C, $[H_2S]aq = 8.3 \times 10^{-4}$ mol/L, 1000rpm, total pressure 1 bar, 1wt% NaCl.

Effect of Temperature

In order to investigate the effect of temperature in the presence of H_2S, experiments were conducted at the same aqueous H_2S concentration, $[H_2S]_{aq}$, using different gas concentrations of H_2S in N_2 at each temperature (30°C, 60°C, and 80°C) to maintain an approximate $[H_2S]_{aq} = 8.3 \times 10^{-4}$ mol/L.

Corrosion rate measured from LPR increased from 1.6 mm/year at 30°C to 5.0 mm/year at 80°C. This change of corrosion rate can be explained from the polarization curves at different temperatures shown in Figure 9. Temperature is known to accelerate most of the chemical, electrochemical and transport processes occurring in the system and both cathodic reactions and anodic currents which were measured increased with increasing temperature. The increase of anodic current is not as significant as the one stemming from cathodic reactions. Water reduction current and the limiting current also increase with increasing temperature.

PHYSICO-CHEMICAL MODEL

Cathodic Reactions

When H_2S is not present in the system, the main cathodic reactions are H^+ reduction:

$$2H^+(aq) + 2e^- \rightarrow H_2(g) \quad (7)$$

which is the most important cathodic reaction in an acidic solution. In the case of mild steel corrosion, this reaction is limited by the rate at which H^+ ions are transported from the bulk solution to the steel surface (mass transfer limitation).

As the availability of H^+ ion decreases, at pH>5 or at lower potentials, the direct reduction of water may become important:

$$2H_2O(l) + 2e^- \rightarrow H_2(g) + 2OH^-(aq) \quad (8)$$

When H_2S is present in the system, the following additional reactions occur:

- H_2S gas dissolves in water to form aqueous H_2S:

$$H_2S(g) \overset{K_{sol(H2S)}}{\Leftrightarrow} H_2S(aq) \quad (9)$$

- Aqueous H_2S is a mild acid which partly dissociates in two steps:

$$H_2S(aq) \overset{K_{H_2S}}{\Leftrightarrow} H^+(aq) + HS^-(aq) \quad (10)$$

$$HS^-(aq) \overset{K_{HS^-}}{\Leftrightarrow} H^+(aq) + S^{2-}(aq) \quad (11)$$

As H_2S is an excellent electron acceptor,[14] the direct reduction of H_2S can also occur as has been experimentally proven in this work:

$$2H_2S(aq) + 2e^- \rightarrow H_2(g) + 2HS^-(aq) \quad (1)$$

This reaction has a limiting current which is controlled by a mass transfer rate from bulk solution to the steel surface, and is sensitive to flow.

Anodic Reaction

Bockris *et al.*[13] proposed the following mechanism of anodic iron dissolution in strong acids (pH<4) which applies to cases when H_2S is not present in the system:

$$Fe + OH^- \Leftrightarrow [FeOH]_{ad} + e^- \quad (12)$$

$$[FeOH]_{ad} \xrightarrow{RDS} [FeOH^+]_{ad} + e^- \quad (13)$$

$$[FeOH^+]_{ad} \Leftrightarrow Fe^{2+} + OH^- \quad (14)$$

This mechanism suggests that the reaction order with respect to OH^- ions is 1, which is valid in acidic solutions; it has also been found that iron dissolution proceeds with little influence of pH for solutions where pH is above approximately 4[13].

In the presence of H_2S, Shoesmith *et al.*[2] proposed

$$Fe + HS^- \Leftrightarrow [FeSH]^-_{ad} \quad (15)$$

$$[FeSH]^-_{ad} \rightarrow [FeSH]^+_{ad} + 2e^- \quad (16)$$

In this mechsnism, two electrons are released in one step, which is not likely to happen. However, the iron dissolution mechanism can be rewritten to appear similar to the one proposed by Bockris *et al.*, this time for solution containing H_2S, as proposed by Ma *et al.*[15] :

$$Fe + HS^- \Leftrightarrow [FeSH]^-_{ad} \quad (17)$$

$$[FeSH]^-_{ad} \Leftrightarrow [FeSH]_{ad} + e^- \quad (18)$$

$$[FeSH]_{ad} \rightarrow [FeSH]^+_{ad} + e^- \quad (19)$$

MATHEMATICAL MODEL

In order to mathematically and numerically describe the physico-chemical model, the measured cathodic and anodic currents reported above are used as a basis.

H^+ Reduction

For H^+ reduction, in order to describe the effect of charge transfer and mass transfer on H^+ reduction, the current density for reduction of H^+ consists of two components: charge transfer current and mass transfer limiting current. Total current density is calculated using a harmonic mean[12]

$$\frac{1}{i_{H^+}} = \frac{1}{i_{\alpha,H^+}} + \frac{1}{i^d_{\lim,H^+}} \tag{20}$$

where i_{H^+} is total current density of H^+ reduction (A/m^2), $i_{\alpha(H^+)}$ is the charge transfer current density (A/m^2), $i^d_{\lim(H^+)}$ is the diffusion limiting current density.

The charge transfer current density can be calculated using the Tafel equation as:

$$i_{\alpha,H^+} = i_{0,H^+} \times 10^{-\frac{\eta}{b_c}} \tag{21}$$

where $i_{0(H^+)}$ is the exchange current density, b_c is the cathodic Tafel slope (V/decade), η is the over potential (V), which is equal to the difference between the applied potential and the reversible potential.

The cathodic Tafel slope b_c can be calculated from:

$$b_c = \frac{2.303RT}{\alpha_c F} \tag{22}$$

According to Bockris, *et al.*,[13] for H^+ reduction, $\alpha_c = 0.5$ giving $b_c \approx 0.120$ V/decade at 30°C. This agreed well with the present findings.

The reversible potential of hydrogen reduction can be calculated as:

$$E_{rev(H^+)} = -\frac{2.303RT}{F} pH - \frac{2.303RT}{2F} \log P_{H_2} \tag{23}$$

where the partial pressure of hydrogen normally is assumed to be close to zero. The only unknown model parameter for calculating the charge transfer current density is the exchange current density, $i_{0(H^+)}$. According to Nesic *et al.*[16], $i_{0(H^+)}$ can be calculated by

$$i_{0,H^+} = i_0^{ref} \left(\frac{C_{H^+}}{C_{H^+ ref}} \right)^{0.5} \times e^{\frac{\Delta H}{R}\left(\frac{1}{T} - \frac{1}{Tref}\right)} \tag{24}$$

where i_0^{ref} is the reference exchange current density at a reference temperature, T_{ref} (K) and reference concentration of H^+. ΔH is the enthalpy of activation for the H^+ reduction reaction (J/mol).

The i_0^{ref} for H^+ reduction was taken as 0.03 A/m^2 at reference temperature 20°C and reference H^+ concentration, 1×10^{-4} mol/L. The enthalpy of activation was taken as 30 kJ /mol[16]. No effect of H_2S on H^+ reduction was found in our experiments.

Limiting Current for H^+ reduction

The diffusion limiting current appearing in Equation **(**20**)** is calculated with:

$$i^d_{\lim,H^+} = k_{m,H^+} F C_{H^+} \tag{25}$$

Where k_{m,H^+} is H^+ mass transfer coefficient (m/s) and c_{H^+} is the bulk concentration of H^+ (mol/m^3).

Mass transfer coefficient of H^+ can be calculated from a rotating cylinder correlation by Eisenberg *et al.* [11]

$$Sh = \frac{k_{m,H^+} d_{RCE}}{D_{H^+}} = 0.0791 \times \mathrm{Re}^{0.7} \times Sc^{0.356} \quad \textbf{(26)}$$

where *Sh* is Sherwood number; d_{RCE}: pipe diameter (m); D_{H+} is diffusion coefficient of hydrogen ion (m^2/s); *Re* is Reynolds number $= \rho u d_{RCE} / \mu$; and *Sc* is Schmidt number $= \mu / \rho D_{H^+}$.

In a dilute solution, the diffusion coefficient of species can be calculated using the Stokes-Einstein equation

$$D_{H^+} = D_{ref(H^+)} \times \frac{T_k}{T_{ref}} \times \frac{\mu_{ref}}{\mu} \tag{27}$$

where D_{ref} is the reference diffusion coefficient at a reference temperature, μ is the water viscosity in kg/m·s and μ_{ref} is the reference viscosity at a reference temperature. $D_{ref(H^+)}$ was taken as 9.31x10^{-9} m^2/s[17] and μ_{ref} was taken as 1.002 kg/(m·s)[18] at reference temperature (293.15 K).

The temperature dependence of water density and water viscosity can be given as:

$$\rho = 1152.3 - 0.5116 \times T_k \tag{28}$$

$$\mu = \mu_{ref} \times 10^{\frac{1.3272(20 - T_c) - 0.001053(20 - T_c)^2}{T_c + 105}} \tag{29}$$

Where T_C, T_K is temperature in °C and Kelvin respectively.

Direct H_2S Reduction

H_2S takes part in the corrosion process in two main ways. Firstly, by dissociation, it can provide an additional source of H^+ which can be reduced. Secondly, H_2S can be directly reduced on steel surface and further increase the corrosion rate.

It has been shown that the current density for direct reduction of H_2S could be limited either by charge transfer or mass transfer. The total current density is given by:

$$\frac{1}{i_{H_2S}} = \frac{1}{i_{\alpha,H_2S}} + \frac{1}{i^d_{\lim,H_2S}} \quad \textbf{(30)}$$

where $i_{H_2S}, i_{\alpha,H_2S}$ *and* $i^d_{\lim,H_2S}$ are total current density, charge transfer current density and mass transfer limiting current density of this reaction in A/m^2, respectively.

Charge transfer current density of this reaction can be calculated using the equation:

$$i_{\alpha,H_2S} = i_{0,H_2S} \times 10^{-\frac{\eta}{b_c}} \quad (31)$$

Tafel Slope

From the experiments, b_c for H_2S reduction in Equation **(**27**)** was found to be close to 120 mV/decade at 30°C, which is the same as for H^+ reduction. The cathodic Tafel slope b_c can be calculated from Equation **(**22**)**.

Exchange Current Density:

From the best fit to experimental results at different concentration of H_2S at pH4, the order n of the reaction with respect to C_{H2S} is found to be:

$$\frac{\partial \log i_{0(H_2S)}}{\partial \log C_{H_2S}} \approx 0.5 \quad (32)$$

The same reaction order of 0.5 was also suggested by J. Kittel *et al.*[19]. It is similar to the one associated with the exchange current density of H^+ reduction. Morris *et al.*[7] and Cheng *et al.*[9] stated that corrosion reaction order with H_2S: n = (log i_{corr}/log[H_2S]) = 0.2. However, i_{corr} includes both contributions from H^+ and H_2S reduction. Under their experimental conditions (pH from 0.75 to 4), the contribution from H^+ is dominant and would not allow an accurate calculation of the H_2S reduction reaction order.

Therefore, the exchange current density should be calculated by

$$i_{0,H_2S} = i_0^{ref} \left(\frac{C_{H_2S}}{C_{H_2S ref}} \right)^{0.5} \left(\frac{C_{H^+}}{C_{H^+ ref}} \right)^{-0.5} \times e^{\frac{\Delta H}{R}(\frac{1}{T} - \frac{1}{Tref})} \quad (33)$$

Where the i_0^{ref} for H_2S reduction is taken as 0.00015 A/m^2 at reference temperature 293.15K and reference H^+ concentration, 1×10^{-4} mol/L and reference H_2S concentration, 1×10^{-4} mol/L. This means that the H_2S reduction rate is about 200 times slower than the H^+ reduction rate (0.03 A/m^2) at the same condition. The enthalpy of activation was taken as 60 kJ/mol from the best fit to experimental results.

Reversible Potential

The two electrochemical reactions: the reduction of H_2S and H^+ are equivalent thermodynamically and have the same reversible potential given by Equation **(**23**)**.

Limiting Current Density

Calculation of limiting current density for H_2S reduction is similar to that for H^+ reduction. The mass transfer limiting current density of this reaction is given by:

$$i^d_{\lim,H_2S} = k_{m,H_2S} Fc_{H_2S} \tag{34}$$

$$Sh = \frac{k_{m,H_2S} d_{RCE}}{D_{H_2S}} = 0.0791 \times \mathrm{Re}^{0.7} \times Sc^{0.356} \tag{35}$$

$$D_{H_2S} = D_{ref(H_2S)} \times \frac{T_k}{T_{ref}} \times \frac{\mu_{ref}}{\mu} \tag{36}$$

Where $D_{ref(H_2S)}$ was taken as 1.61×10^{-9} m^2/s at reference temperature (293.15 K).[20] The concentration of H_2S can be calculated by:

$$C_{H_2S} = K_{sol(H_2S)} \times p_{H_2S} \tag{37}$$

Where p_{H2S} is partial pressure of H_2S in bar, $K_{sol(H_2S)}$ is Henry's constant in mol/bar which is given by[21]

$$K_{sol(H_2S)} = 10^{-\left(634.27+0.2709T_k-0.11132\times10^{-3}T_k^2-\frac{16719}{T_k}-261.9\log T_k\right)} \tag{38}$$

Water Reduction

Since water molecules are present in almost unlimited quantities at the metal surface, it can be assumed that at all times the reduction rate of H_2O is controlled by the charge-transfer process and, hence, the Tafel equation is used:

$$i_{H_2O} = i_{0,H_2O} \times 10^{\frac{\eta}{b_c}} \tag{39}$$

Tafel slope in all experiments at 30°C was found to be close to 120 mV/decade, which is the same as that for H^+ reduction. Tafel slope for H_2O reduction is given by Equation (22).

Since the electrochemical reduction of H_2O and H^+ are equivalent thermodynamically, the reversible potential and H_2O reduction were assumed to be the same as for H^+ reduction, which is calculated by Equation (23).

Exchange Current Density:

When H_2S is not present, the exchange current density for H_2O reduction is given by

$$i_{0,H_2O} = i_0^{ref}\left(\frac{C_{H^+}}{C_{H^+_{ref}}}\right)^{-0.5} e^{\frac{\Delta H}{R}(\frac{1}{T}-\frac{1}{Tref})} \quad \textbf{(40)}$$

The i_{0ref} for H_2O reduction was taken as 2×10^{-5} A/m^2 at reference temperature 293.15K and reference H^+ concentration 1×10^{-4} mol/L. The enthalpy of activation was taken as 30 kJ/mol.[12]

When H_2S is present, apparently it can retard the H_2O reduction, resulting in rates about 20 times lower than that seen in environments without H_2S. From the current experimental results, the reaction order log $i_{0,H2O}$/log[H_2S] is close to 0.1. The exchange current density is given by

$$i_{0,H_2O} = i_0^{ref}\left(\frac{C_{H^+}}{C_{H^+_{ref}}}\right)^{-0.5}\left(\frac{C_{H_2S}}{C_{H_2Sref}}\right)^{-0.1} e^{\frac{\Delta H}{R}(\frac{1}{T}-\frac{1}{Tref})} \quad \textbf{(41)}$$

In an H_2S environment, the i_0^{ref} for H_2O reduction was taken as 1×10^{-6} A/m^2 at reference temperature 293.15K, the reference H^+ concentration of 1×10^{-4} mol/L, and the reference H_2S concentration of 1×10^{-4} mol/L. The enthalpy of activation was taken as 90 kJ/mol from the best fit to experimental results, which would suggest that H_2O reduction in an H_2S environment is more sensitive to temperature.

Anodic Dissolution of iron

In the present experiments, the anodic dissolution of iron was under charge transfer control. Thus, pure Tafel behavior can be assumed close to the corrosion potential

$$i_{Fe} = i_{0,Fe}\times10^{\frac{\eta}{b_a}} \quad \textbf{(42)}$$

The Tafel slopes of anodic reaction in H_2S environment or environment without H_2S are all close – in the range 40-50 mV/decade. H_2S did not have any effect on the Tafel slope, so for anodic iron dissolution, Tafel slope is given as:

$$b_a = \frac{2.303RT}{\alpha_a F} \quad \textbf{(43)}$$

According to Bockris, *et al.*[13], the apparent symmetry coefficient for the anodic reaction of Fe dissolution was taken as 1.5, giving b_a = 40 mV at 30°C, which is close to our experimental results. The reversible potential of X-65 steel was taken[12] to be – 0.488 V.

Exchange current density:

When H_2S is not present, according to the mechanism proposed by Bockris *et al.*[13], the reaction order with respect to OH^- ions is 1, which is valid in acidic solutions; it has been found that iron dissolution proceeds with little influence of pH for solutions above approximately pH4. It is assumed that the exchange current density is proportional to the surface coverage of OH^- (θ_{OH^-}) and it that it follows the Frumkin adsorption model:

$$i_{0,Fe} = i^*_{0,Fe}\theta_{OH^-} e^{\frac{\Delta H}{R}(\frac{1}{T}-\frac{1}{Tref})} \quad (44)$$

$$\mathrm{K}_1 C_{OH^-} = \frac{\theta_{OH^-}}{1-\theta_{OH^-}} e^{(-f\theta_{OH^-})} \quad (45)$$

According to the current experimental results and Bockris *et al.*[13], the best-fit values in Equation (44) and (45) are $i^*_{0,Fe}$ = 0.25, K_1 = 1.56×10^9 and *f* = 3.83. Actually when *f* is equal to 0, the Frumkin adsorption model becomes the Langmuir adsorption model. The reference temperature is 293.15K. The activation energy ΔH was set to be 37.5 kJ/mol, which is taken from the finding of Nesic *et al.*[16]

The concentration of OH^- can be calculated by

$$C_{OH^-} = \frac{K_{wa}}{C_{H^+}} \quad (46)$$

K_{wa} is the equilibrium constant of the water dissociation reaction, which can be calculated by:[22]

$$K_{wa} = 10^{-(29.3868-0.0737549\times T_k+7.47881\times 10^{-5}\times T_k^2)} \quad (47)$$

When H_2S is present, according to the mechanism proposed previously, Equations (17), (18), and (19), the exchange current density for iron dissolution is related to HS^- concentration. Even at low concentrations of H_2S, such as 100 ppm H_2S (0.1mbar) and pH4, the concentration of HS^- is much higher (1×10^{-8} mol/L) than the concentration of OH^- (1×10^{-10} mol/L). Therefore, the contribution of OH- to the anodic reaction was ignored. It can be assumed that the exchange current density is only related to the surface coverage of HS^- (θ_{HS^-}) and that it follows the Langmuir adsorption model:

$$i_{0,Fe} = i^{*'}_{0,Fe}\theta_{HS^-} e^{\frac{\Delta H}{R}(\frac{1}{T}-\frac{1}{Tref})} \quad (48)$$

$$\theta_{HS^-} = \frac{K_2 C_{HS^-}}{1+K_2 C_{HS^-}} . \quad (49)$$

The best fit values in Equation (48) and (49) for $i^{*'}_{0,Fe}$ =0.33, K_2=3.5×10^6. The reference temperature is 293.15 K. The activation energy ΔH was assumed to be the same as for an environment without H_2S (37.5 kJ/mol). C_{HS^-} is the concentration of HS^-, which is given by

$$C_{HS^-} = \frac{K_{H2S} C_{H_2S}}{C_{H^+}} \quad (50)$$

K_{H2S} is the equilibrium constant for the first dissociation of H_2S, which can be calculated by:[23]

$$K_{H_2S} = 10^{782.43945+0.361261 T_k - 1.6722\times 10^{-4} T_k^2 - \frac{20565.7315}{T_k} - 142.741722 \ln T_k} \quad (51)$$

Implementation of the Model

The model requires as input: temperature, pH, P_{H2S}, and the hydrodynamic parameters: in this case the rotating cylinder diameter, and the rotational velocity. The corrosion potential then can be calculated by solving the charge balance equation:

$$\sum i_a = \sum i_c \qquad \textbf{(52)}$$

which here takes the form:

$$i_{Fe} = i_{H_2S} + i_{H^+} + i_{H_2O} \qquad \textbf{(53)}$$

Once the corrosion potential is known, the corrosion current and rate can be found from the anodic current (or total cathodic current) at the corrosion potential. The individual and total cathodic and anodic curves, and predicted potentiodynamic sweeps can be generated.

MODEL VALIDATION

Performance of the model was validated by comparing the predictions with experimental results described above.

Effect of pH_2S

Figure 10 shows that the predicted corrosion rates from the electrochemical model are in good agreement with experimental results, which suggests that the electrochemical model captured the main effects of H_2S corrosion of mild steel in the absence of iron sulfide layers.

Figure 12, Figure 13, Figure 14 show cathodic and anodic polarization curves changing with H_2S concentration for the different pH environments. The model prediction captures the anodic reaction change in the low pH environment (Figure 13, for pH3) due to the HS^- adsorption and the cathodic reaction change in high pH environments (Figure 14, for pH5) due to the additional cathodic reaction: H_2S reduction. Predicted potentiodynamic sweeps are in good agreement with experimental results for individual reactions generated with the present model.

Using the model, the cathodic polarization curves can be deconvoluted to show three individual reduction reactions (H^+ reduction, H_2S reduction and H_2O reduction). It can be seen for example that when increasing the H_2S concentration, the H^+ reduction doesn't change, that the H_2S reduction curve moves to the higher values at the right and that the H_2O reduction changes only a little; see Figure 12, Figure 13, and Figure 14.

Effect of Flow rate

The effect of flow rate on both cathodic reaction and anodic reaction at 1% and 10% H_2S is depicted in Figure 15 and Figure 16. Increasing rotating speed does not affect the anodic reaction and H_2O reduction, but accelerates the cathodic reaction due to the increase of mass transfer limiting current related to H^+ reduction and H_2S reduction. Except for the case of the limiting current density at 200 rpm rotating speed, all the predicted polarization curves agree well with the experimental results.

Corrosion rate predictions are shown in Figure 11. The predicted corrosion rates are close to the experimental results.

Effect of pH

Comparison between predicted polarization curves and experimental polarization curves in solution without H_2S are shown in Figure 17. A good agreement is found at each pH. From Figure 17, H^+ reduction curves shift to the higher values on the right with pH decrease while anodic reaction curves move to lower values on the left with pH decrease.

When 100ppm H_2S is present, the prediction of polarization curves is shown in Figure 18. Due to the low concentration of H_2S in solution, no obvious effect on cathodic polarization curve was observed. As mentioned previously, anodic reaction is related the HS^- concentration. At the same gas concentration of H_2S, [HS^-] is inversely proportional to the pH, so the anodic reaction rate increases with pH increase. The experimental and predicted polarization curves were found to be in very good agreement.

For 10% H_2S present, the comparison of the predicted polarization curves with the experimental results is shown in Figure 19. It is evident that the model prediction is in good agreement with the experimental data at each pH. H_2S concentration is higher so H_2S reduction can affect the cathodic polarization curves significantly. Anodic polarization curves are not sensitive to pH in Figure 19 due to the high concentration of HS^-.

Corrosion rate prediction at different pH is shown in Figure 20. The electrochemical model predictions are in good agreement with experimental results, which means the electrochemical model captured the main features of H_2S corrosion at different pH.

Effect of temperature

The effect of temperature on both cathodic reaction and anodic reaction at [H_2S] = 8.3×10^{-4} M is depicted in Figure 22. Increasing temperature has a small influence on the anodic reaction, but accelerates the cathodic reaction greatly. H^+ reduction, H_2S reduction and H_2O reduction rate increase with temperature increase. All the predicted sweeps agree with experimental results well.

Corrosion rate predictions are shown in Figure 21. This electrochemical model is captures well the corrosion rate change with temperature.

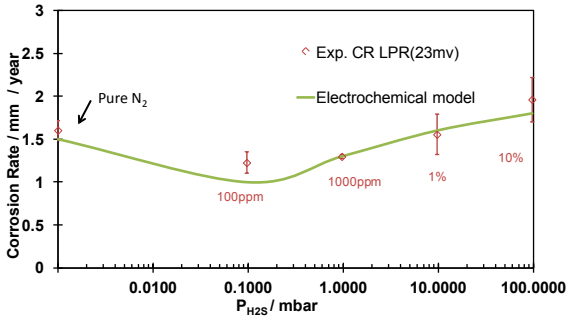

Figure 10. Comparison of corrosion rate predictions with LPR experimental results at pH4 and different H_2S concentration, total pressure=1.0 bar, 1000rpm 30°C, B = 23 mV/ decade.

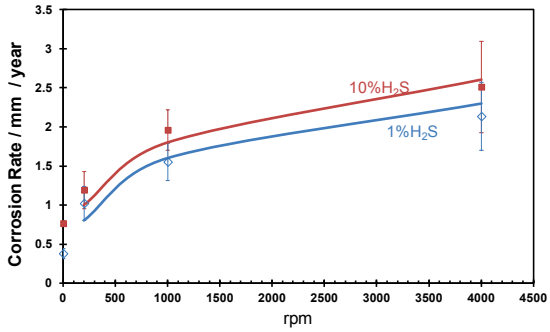

Figure 11. Comparison of predicted corrosion rate with LPR experimental results at different rotational speed, pH4, total pressure=1.0 bar, 30°C, points: experimental results, solid lines: predicted curves, B = 23 mV/ decade.

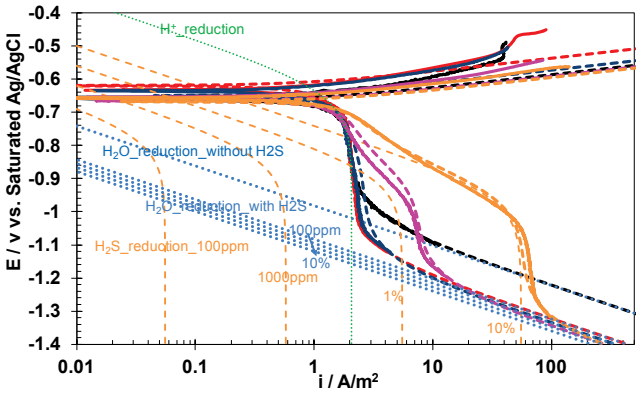

Figure 12. Comparison of predicted polarization curves with experimental results at different H_2S concentration, pH4, total pressure=1.0 bar, 1000rpm, 30°C. Solid line: experimental curves. Dashed line: predicted curves. Black: 0ppm H_2S, Red: 100ppm H_2S, Dark blue: 1000ppm H_2S, Pink: 1%H_2S, purple: 10%H_2S.

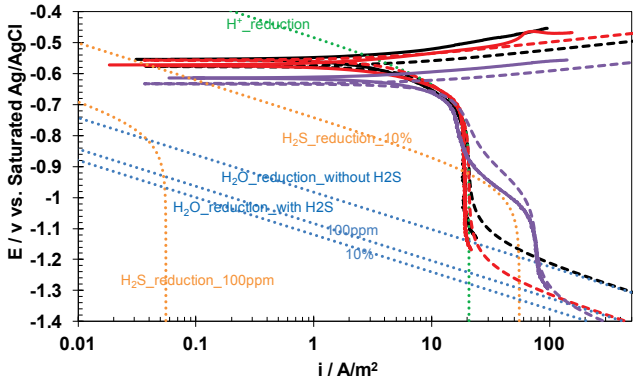

Figure 13. Comparison of predicted polarization curves sweeps with experimental results at different H_2S concentration, pH3, total pressure=1.0 bar, 1000rpm, 30°C. Solid line: experimental curves. Dashed line: predicted curves. Black: 0ppm H_2S, red: 100ppm H_2S, purple: 10% H_2S.

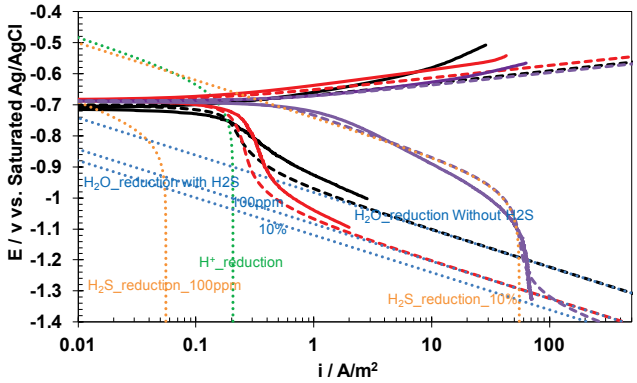

Figure 14. Comparison of predicted polarization curves with experimental results at different H_2S concentration, pH5, total pressure=1.0 bar, 1000rpm, 30°C. Solid line: experimental curves. Dashed line: predicted curves. Black: 0ppm H_2S, red: 100ppm H_2S, purple: 10% H_2S.

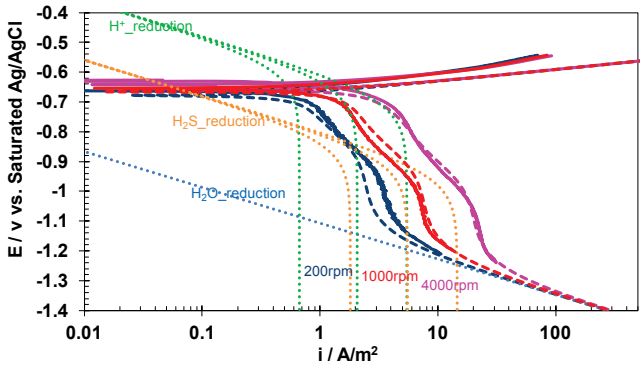

Figure 15. Comparison of predicted polarization curves with experimental results at different rotated speed, pH4, 1% H_2S, total pressure=1.0 bar, 30°C. Solid line: experimental curves. Dashed line: predicted curves. Dark: 200rpm, red: 1000rpm, pink: 4000rpm.

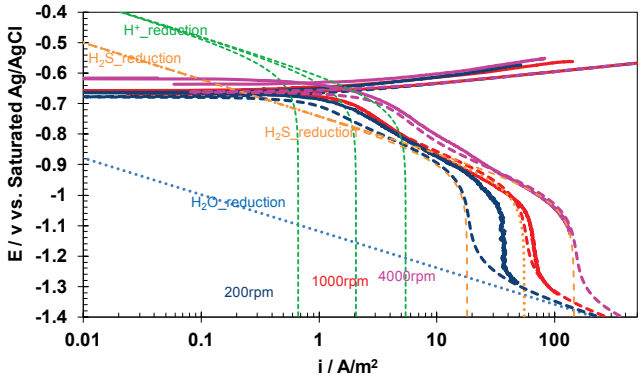

Figure 16. Comparison of predicted polarization curves with experimental results at different rotated speed, pH4, 10% H_2S, total pressure=1.0 bar, 30°C. Solid line: experimental curves. Dashed line: predicted curves. Dark blue: 200rpm, red: 1000rpm, pink: 4000rpm.

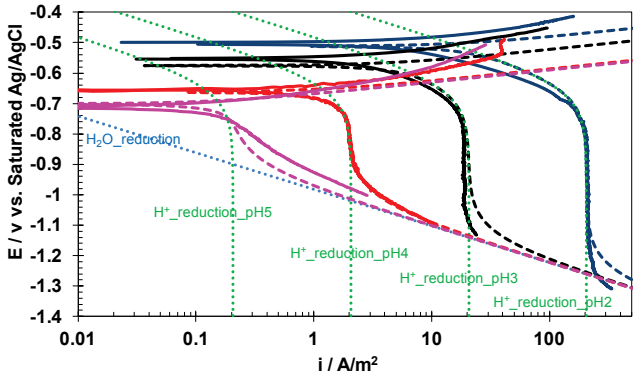

Figure 17. Comparison of predicted polarization curves with experimental results at different pH, 1000rpm, 0ppm H_2S (N_2), total pressure=1.0 bar, 30°C. Solid line: experimental curves. Dashed line: predicted curves. Pink: pH5, Dark blue: pH2, black: pH3, red: pH4, pink: pH5.

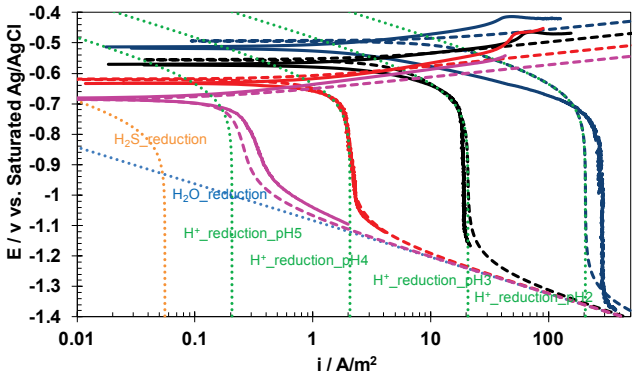

Figure 18. Comparison of predicted polarization curves with experimental results at different pH, 1000rpm, 100ppm H_2S /N_2, total pressure=1.0 bar, 30°C. Solid line: experimental curves. Dashed line: predicted curves. Pink: pH5, Dark blue: pH2, black: pH3, red: pH4, pink: pH5.

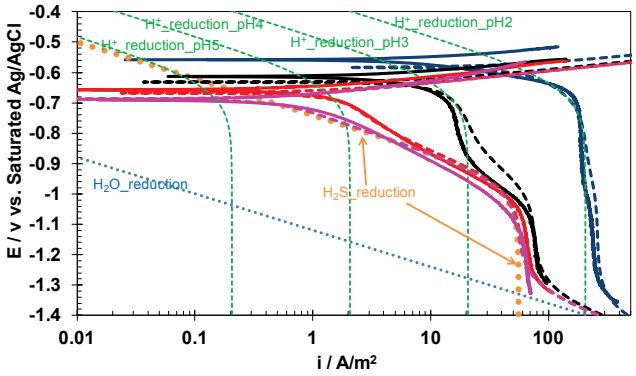

Figure 19. Comparison of predicted polarization curves with experimental results at different pH, 1000rpm, 100ppm H_2S /N_2, total pressure=1.0 bar, 30°C. Solid line: experimental curves. Dashed line: predicted curves. Pink: pH5, Dark blue: pH2, black: pH3, red: pH4, pink: pH5.

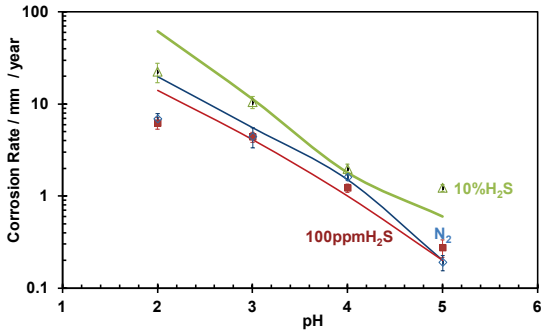

Figure 20. Comparison of predicted corrosion rate with experimental results at different pH, different H_2S concentration, 1000rpm, total pressure=1.0 bar, 30°C, point: experimental results, solid line: predicted curves. LPR constant B = 23 mV/ decade.

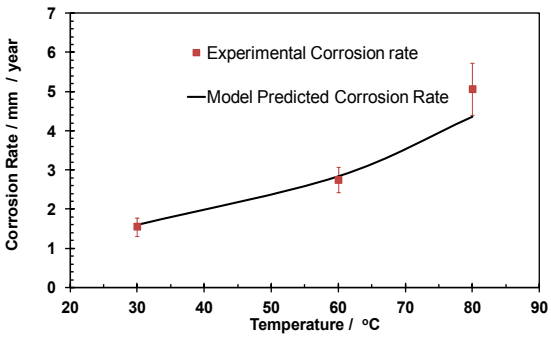

Figure 21 Comparison of predicted corrosion rate with experimental results at different temperature, 1000rpm, [H_2S] = 8.3×10^{-4}mol/L, total pressure=1.0 bar, 30°C, Point: experimental results, solid line: predicted curves. LPR constant B = 23 mV/ decade.

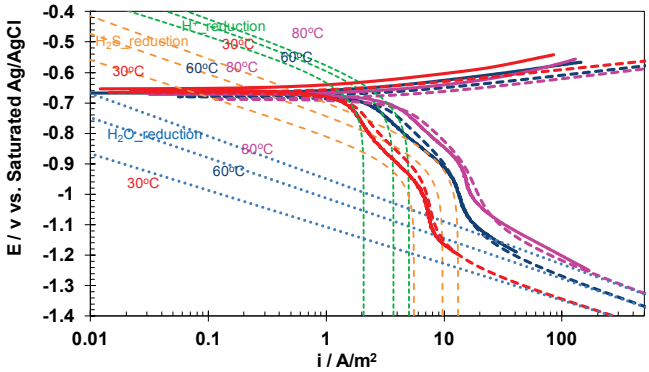

Figure 22. Comparison of predicted polarization curves with experimental results at different temperature, 1000rpm, [H_2S] = 8.3×10^{-4}mol/L, total pressure=1.0 bar, 30°C. Solid line: experimental curves. Dashed line: predicted curves. Red: 30°C, Dark blue: 60°C, pink: 80°C.

CONCLUSIONS

- The presence of H_2S affects both cathodic reactions and the anodic reaction.
- In a solution with $[H_2S]_{aq}$, an additional cathodic reaction, direct H_2S reduction, was clearly observed. This reaction is flow sensitive and a mass transfer limiting current density was identified. The Tafel slope was observed to be close to 120 mV/decade at 30°C. The reaction order with C_{H2S} is estimated to be close to 0.5.
- A retardation effect of $[H_2S]_{aq}$ on H_2O reduction was observed at all experimental conditions, even at relatively high H^+ concentrations seen at pH2.
- Both an acceleration and a retardation effect of H_2S on the anodic dissolution of iron were observed in acidic solutions. This effect is related the chemisorption of HS^- ions. The effect can be explained by the Langmuir adsorption model. The Tafel slope for the anodic dissolution of iron was 40~50mV/ decade. When [HS^-] reached a critical value, the anodic reaction current reached a maximum and became independent of both [HS^-] and pH.
- A new electrochemical model has been developed that can be used to simulate the effect of pH_2S, flow, temperature and pH on corrosion of mild steel in an H_2S environment in the absence of iron sulfide layers.

ACKNOWLEDGEMENTS

The authors would like to express sincere appreciation to the following industrial sponsors for their financial support and direction: BG Group, BP, Champion Technologies, Chevron, Clariant Oil Services, ConocoPhillips, Encana, ENI S.P.A., ExxonMobil, WGIM, NALCO Energy Services, Occidental Oil Company, Petrobras, PETRONAS, PTT, Saudi Aramco, INPEX Corporation, Total, TransCanada.

REFERENCES

[1] S. N. Smith and M. W. Joosten, "Corrosion of carbon steel by H_2S in CO_2 containing oilfield environments," in *CORROSION/2006,* paper no. 06115, NACE International, 2006.

[2] D. W. Shoesmith, P. Taylor, M. G. Bailey and D. G. Owen, "The formation of ferrous monosulfide polymorphs during the corrosion of iron by aqueous hydrogen sulfide at 21°C," *J. Electrochem. Soc.,* vol. 127, pp. 1007-1015, May, 1980.

[3] W. Sun, "Kinetics of iron carbonate and iron sulfide scale formation in carbon dioxide/hydrogen sulfide corrosion," Ph.D. dissertation, Dept. Chem. Eng, Ohio University, Athens, OH, USA, 2006.

[4] R. H. Hausler, "Contribution to the understanding of H_2S corrosion," in *CORRROSION/2004,* paper no.04732, NACE International, 2004.

[5] S. N. Smith and J. L. Pacheco, "Prediction of corrosion in slightly sour environments," in *CORROSION/2002,* paper no. 02241, Denver, CO, NACE International, 2002.

[6] S. N. Smith, "A proposed mechanism for corrosion in slightly sour oil and gas production," in *12th International Corrosion Congress: Corrosion Control for Low-Cost Reliability Conference,* paper no. 385, Houston, Texas, USA, NACE International, September 19-24, 1993.

[7] D. R. Morris, L. P. Sampaleanu and D. N. Veysey, "The corrosion of steel by aqueous solutions of hydrogen sulfide," *J. Electrochem. Soc.,* vol. 127, pp. 1228-1235, 1980.

[8] Z. A. Iofa, V. V. Batrakov and Cho-Ngok-Ba, "Influence of anion adsorption on the action of inhibitors on the acid corrosion of iron and cobalt," *Electrochim. Acta,* vol. 9, pp. 1645-1653, 12, 1964.

[9] X. L. Cheng, H. Y. Ma, J. P. Zhang, X. Chen, S. H. Chen and H. Q. Yang, "Corrosion of iron in acid solutions with hydrogen sulfide," *Corrosion,* vol. 54, pp. 369-376, May, 1998.

[10] W. Sun and S. Nesic, "A mechanistic model of uniform hydrogen Sulfide/Carbon dioxide corrosion of mild steel," *Corrosion,* vol. 65, pp. 291-307, 2009.

[11] M. Eisenberg, C. W. Tobias and C. R. Wilke, "Ionic mass transfer and concentration polarization at rotating electrodes," *Journal of the Electrochemical Society,* vol. 101, pp. 306-320, January 01, 1954.

[12] S. Nesic, J. Postlethwaite and S. Olsen, "An electrochemical model for prediction of corrosion of mild steel in aqueous carbon dioxide solutions," *Corrosion,* vol. 52, pp. 280-294, 1996.

[13] J. O. Bockris, D. Drazic and A. R. Despic, "The electrode kinetics of the deposition and dissolution of iron," *Electrochim. Acta,* vol. 4, pp. 325-361, 8, 1961.

[14] D. Rickard and G. W. Luther, "Chemistry of iron sulfides," *Chem. Rev.,* vol. 107, pp. 514-562, 2007.

[15] H. Ma, X. Cheng, G. Li, S. Chen, Z. Quan, S. Zhao and L. Niu, "The influence of hydrogen sulfide on corrosion of iron under different conditions," *Corros. Sci.,* vol. 42, pp. 1669-1683, 10, 2000.

[16] M. Nordsveen, S. Nesic, N. Nyborg and A. Stangeland, "A mechanistic model for carbon dioxide corrosion of mild steel in the presence of protective iron carbonate Films Part 1: Theory and verification," *Corrosion,* vol. 59, 2003.

[17] P. W. Atkins, Ed., *Physical Chemistry.* Oxford, England: Oxford University Press, 1982.

[18] R. C. Weast, Ed., *Handbook of Chemistry & Physics.* Boca Raton, FL: CRC Press Inc., 1985.

[19] J. Kittel, F. Ropital, F. Grosjean, E. M. M. Sutter and B. Tribollet, "Corrosion mechanisms in aqueous solutions containing dissolved H2S. part 1: Characterisation of H2S reduction on a 316L rotating disc electrode," *Corros. Sci.,* vol. 66, pp. 324-329, 1, 2013.

[20] R. H. Perry, D. W. Green and J. O. Maloney, "Perry's chemical engineers' handbook," 1984.

[21] O. M. Suleimenov and R. E. Krupp, "Solubility of hydrogen sulfide in pure water and in NaCl solutions, from 20 to 320°C and at saturation pressures," *Geochim. Cosmochim. Acta,* vol. 58, pp. 2433-2444, 6, 1994.

[22] Y. K. Kharaka, W. D. Gunter, P. K. Aggarwal, E. H. Perkins and J. D. Dedraal, "SOLMINEQ. 88 - A computer program for geochemical modeling of water--rock interactions," *United States Geological Survey Water-Resources Investigation Report,* pp. 88-4227, 1988.

[23] O. M. Suleimenov and T. M. Seward, "A spectrophotometric study of hydrogen sulphide ionisation in aqueous solutions to 350°C," *Geochim. Cosmochim. Acta,* vol. 61, pp. 5187-5198, 12, 1997.